Green Chemistry

Additive Manufacturing via Protein Denaturation

Journal:	*Green Chemistry*
Manuscript ID	GC-COM-06-2024-002932.R1
Article Type:	Paper
Date Submitted by the Author:	30-Jul-2024

Complete List of Authors:	Lee, Chang-Uk; University of Wisconsin-Madison, Chemistry Kim, SungJune; University of Wisconsin-Madison, Chemistry Dietrich, Rachel; University of Wisconsin-Madison, Department of Food Science Girard, Audrey; University of Wisconsin-Madison, Department of Food Science Boydston, Andrew; University of Wisconsin-Madison, Chemistry; University of Washington,

ARTICLE

Additive Manufacturing via Protein Denaturation

Chang-Uk Lee[a]; Sung June Kim[a]; Rachel B. Dietrich[b]; Audrey Girard[b]; Andrew J. Boydston[a,c,d*]

Received 00th January 20xx,
Accepted 00th January 20xx

DOI: 10.1039/x0xx00000x

We report vat-based additive manufacturing (or, 3D printing) that leverages protein denaturation as the sole curing mechanism. The approach avoids the use of acrylates, which are often toxic and hazardous materials. Instead, additive manufacturing by protein denaturation uses techniques that enable control over the location of photothermal transduction such that protein aggregation drives the conversion of aqueous resin into solid parts. In this way, we introduce a safe and sustainable approach to production of complex three-dimensional objects that maintain full biodegradability.

Introduction

Considering the accumulation of wastes from petroleum-based plastics as well as a need to move toward a circular economy for material recycling, there is high demand for bioplastic materials that display desirable structural and functional integrity. The definition of 'bio' in bioplastics includes polymers synthesized from renewable sources (biomass), polymers extracted from biomass, (bio)degradable polymers, materials produced through biological processes, and combinations thereof.[1] Despite high demand for bioplastics, it has been challenging to achieve structures, properties, and production costs of bioplastics that are comparable to those of legacy petroleum-based plastics.[2–6] Polylactic acid (PLA) and polyhydroxyalkanoates (PHAs) are the most promising alternatives to traditional plastics with production at a large scale (13.9% of 2.11 million tons of bioplastics produced in Europe, 2019).[5] There are, however, drawbacks including incomplete degradation of PLA in water and long (months) processes to fully degrade at elevated temperatures (58 °C).[7] Among other bioplastics, which include starch- and cellulose-based plastics, proteins have drawn considerable attention as structural and functional bioplastics due to their feasibility of feedstocks, such as microbial, plant, and animal sources, as well as their superior oxygen barrier properties in comparison with traditional plastics.[7,8] Implementation of protein-based materials, however, remains challenging due to their low processibility into three dimensional (3D) structural components, as well as poor mechanical properties of parts made from protein build materials.[2]

Additive manufacturing (AM) with protein feedstocks has been investigated to achieve production of 3D bioplastic parts with impressive structural complexity and functionality. For example, Nelson and co-workers reported vat photopolymerization (VP) of methacroylated bovine serum albumin (BSA).[2–4] They demonstrated the creation of complex 3D structures from BSA-based resins that displayed good mechanical toughness, strain-dependent mechanical behaviour, and shape-memory capabilities. In their studies, to leverage the geometric freedom provided by VP AM, they introduced chemical modifications to BSA to impart photocurable reactivity via pendant methacrylate groups. In other examples, researchers have used extrusion-based AM methods such as direct ink writing (DIW) with rheological modifiers to achieve AM of protein-based formulations.[8–11] Liu et al. reported DIW AM of egg white proteins (EWPs) formulations containing gelatin, cornstarch, or sucrose in addition to EWPs.[11] Phuhongsung et al. reported AM of mixtures of soybean protein isolate along with k-carrageenan as a rheological modifier.[9] The geometric complexity of the parts produced via DIW in those studies was limited compared to VP, which is generally regarding as offering standout geometric freedom amongst AM techniques.

[a] *Department of Chemistry, University of Wisconsin, Madison, Wisconsin 53706, USA.*
[b] *Department of Food Science, University of Wisconsin, Madison, Wisconsin 53706, USA.*
[c] *Department of Chemical & Biological Engineering, University of Wisconsin, Madison, Wisconsin 53706, USA.*
[d] *Department of Materials Science & Engineering, University of Wisconsin, Madison, Wisconsin 53706, USA.*
Electronic Supplementary Information available. See DOI: 10.1039/x0xx00000x

Notably, thermal denaturation of proteins is one of the major processing methods to produce edible films,[12–14] as well as meat substitutes with palatable textures from plant proteins.[15] Heat triggers unfolding of proteins and modification of their three-dimensional structures, exposing internal sulfhydryl (SH) and hydrophobic groups, which subsequently promote intermolecular disulfide bonding and hydrophobic interactions.[13–15] Upon cooling, proteins enter a solidification phase involving inter- and intramolecular aggregation of amino acid chains. Further aggregation and crosslinking into fibrous assemblies often accompanies the decreasing solubility and formation of solid materials.[15] We envisioned using the protein denaturation process as the liquid-to-solid curing method to create deliberate 3D structures (Figure 1). In this way, an ability to pattern thermal energy would lead to aggregation-based curing of proteins without requiring chemical modifications of the protein structure, such as (meth)acroylation, or complex resin formulations. Recently, we disclosed a method of AM that was specifically designed to use light input and photothermal transduction to create 3D parts via thermal curing. The method, termed heating at a patterned photothermal interface (HAPPI), operates similar to VP except that light does not penetrate into the vat and photochemical processes are largely irrelevant. Instead, light is rapidly converted to thermal energy at the build layer due to a photothermal plate that lines the bottom of the resin vat.[16,17] In this study, we report additive manufacturing via protein denaturation (AMPD) of globular proteins, including BSA and EWPs, via HAPPI AM without requiring any chemical modification of the proteins or exogenous rheological modifiers.

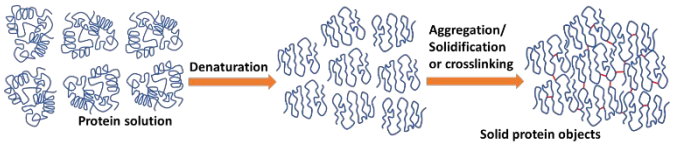

Figure 1 Idealized scheme showing denaturation and aggregation/solidification or crosslinking from protein solution to solid objects.

Experimental

Materials

BSA was purchased from Nova Biologics, Inc., and used as received. Dried EWPs (type H-40) containing 80% protein were donated by Wabash Valley Produce, Inc. and used as received. Tris(2-carboxyethyl)phosphine hydrochloride (TCEP), pepsin (2,500 units/mg), bromothymol blue sodium salts, IR-806, and glycerol were purchased from Sigma-Aldrich and used as received.

Resin formulation

For HAPPI AM with a diode laser, aqueous BSA solution was prepared in DI water at 35 wt% BSA (e.g., 43 g of BSA in 80 mL of water). For HAPPI AM using DLP equipment, BSA (43 g) was dissolved in 68 mL of pH 6.6 citrate-phosphate buffer solution at 35 wt% with addition of 12 mL of 100 mM TCEP solution to obtain a 15 mM final TCEP solution. The buffer solution was prepared by mixing 27 mL of 0.1 M aqueous citric acid and 72 mL of 0.2 M aqueous sodium phosphate dibasic. Aqueous solutions of photothermal dyes (25 mg/mL of bromothymol blue sodium salt in DI water) for DLP AM were added into BSA solutions at 0.1 wt% relative to the entire resin solution. Aqueous solution of photothermal dyes, IR-806 (10 mg/mL), for AM with diode laser were added into BSA solution at 0.15 wt% relative to the entire resin solution. For BSA solution in water/glycerol mixture, BSA (46 g) was dissolved in a mixture of 62 mL DI water and 23 g of glycerol (glycerol/protein = 0.5 w/w).

AMPD

For HAPPI AM with a diode laser, we used the previously reported HAPPI setup.[16] We used a commercial vat typical of a DLP 3D printer, which had a square prism (370 × 370 mm^2, void: 300 × 300 mm^2). The open bottom of the vat was covered by a black grill mat (0.2-mm thickness). For HAPPI AM with a diode laser, Repetier-Host was used to load STL files, slice, and execute the printing. The STL files were converted to G code files using Prusa slicer. The infill pattern was a grid at 95% density. A diode laser with a wavelength of 808 nm was purchased from Opto Engine LLC (Midvale, UT, USA). The laser light was directed through a fibre optic cable and a collimator creating a 550-µm beam diameter. The distance between the collimator of the laser and the bottom of the vat was fixed at 15 mm. The major print speed was 1200 mm/min for dogbones and 900 mm/min for gyroids. For HAPPI DLP, the DLP projector was purchased from ViewSonic (model: PA503W). The distance between the projector and grill mat was 11 cm. A focal lens was put on the projector lens to improve resolution while maintaining light intensity. For photothermal vat printing using IR-806 (no grill mat), a common FEP film (0.15-mm thickness) was used with the DLP projector, and a PFE film (with 0.25-mm thickness, CS Hyde Company) was used with the diode laser.

Biodegradation

Procedures for biodegradation assays of printed BSA cylinders were conducted according to Smith, et al. (37 °C in a shaking incubator at 137 rpm).[2] Pepsin solution as an incubation medium was prepared by dissolving pepsin at 3.2 g/L in 0.1 M aqueous HCl.[2] One distinguishing point from their studies is that we replaced the pepsin solution at 2-day intervals to maintain maximum enzymatic activities of pepsin. Three groups of four cylinders (20 × 20 × 6 mm^3) were printed by HAPPI DLP. Three cylinders were evaluated for each time point (zero, 5 days, 10 days, and at full degradation) both with and without post-curing at 120 °C for 3 hours. Samples were taken out of the pepsin solution and dried in the air for 3 days, and then under vacuum for 1 h before measuring the remaining dry mass. Reported values are the averages ± one standard deviation for three replicate measurements.

Instruments

Differential scanning calorimetry (DSC) studies were conducted on a TA DSC Q200 calorimeter under nitrogen. Aqueous protein solutions at 35 wt% were sealed in an

aluminium pan, and heat flow was recorded while heating at 10 °C/min using DI water as a reference. The moisture content of each dogbone after tensile tests was measured by thermogravimetric analysis (TGA) conducted on a TA TGA Q50 by holding the sample at 100 °C for 100 minutes under nitrogen. Kinematic viscosities (ν) of BSA solutions at 35 wt% were measured using a capillary viscometer (IIc without glycerol, IIIc with glycerol), at 27°C with SCHOTT viscosity measuring units, AVS 360. Viscosity was calculated as ν = Kt where K is the equipment calibration constant, 0.3106 mm^2s^{-2} for IIc or 2.987 mm^2s^{-2} for IIIc, and t is the measured flow time in seconds. The flow time was measured three times, and the average viscosity is reported ±one standard deviation. Samples for density measurements and scanning electron microscopy (SEM) were prepared by HAPPI AM of a rectangular prism (20 × 20 × 15 mm^3), cut into four pieces (10 × 10 ×15 mm^3), and then dried open air for three days or until constant mass. The average densities of three samples were measured by recording masses using the analytical balance and calculating volumes based on the dimensions determined using a digital caliper. SEM imaging was conducted using a Zeiss Gemini SEM 450 at an accelerating voltage of 5 kV. Samples for SEM were sputter-coated with 5- or 10-nm thick platinum.

Uniaxial tensile testing was conducted using the MTS Criterion Model 43 with a 50-kN load cell at an extension rate of 5 mm/min.[2] ASTM D638 type V samples for tensile testing were prepared by HAPPI AM. After printing, samples without glycerol were treated with tannic acid solution ([tannic acid] = 300 mg/mL) for three days,[2] dried in ambient conditions for 5 h, and then heated in the oven at 50 ˚C for 30 minutes and then at 100 ˚C for 30 minutes under mild pressure to prevent any warping while drying. Samples with glycerol were dried in ambient conditions for two weeks. We note that ambient conditions were recorded as 21 ± 1 °C with 33 ± 15% humidity across the 6 months of the studies. Post-thermal curing was done in an oven at 120 °C for 3 h. Prior to post-curing, we dried printed dogbones since excessive remaining moisture inside the dogbones produced bubbles during post-curing. Prior to tensile testing, dogbones of BSA (no glycerol) with or without post-curing were hydrated by immersing the samples in DI water for 15 h. Otherwise, samples tended to break when being secured in the grips for tensile testing. For aging studies, BSA samples with glycerol without post-curing were stored in ambient conditions and evaluated at two weeks, one month, two months, and three months. Dogbones of BSA with glycerol after post-curing were tested after 2 days, one month, two months, and three months. Compressive tests were done with the MTS machine at 1.3 mm/min of crosshead velocity.[2] Cylinders with 20-mm diameter and 12-mm height for compressive testing were prepared by HAPPI AM. Dynamic mechanical analyses (DMA) on rectangles of BSA with and without glycerol were done on a PerkinElmer DMA 8000. Samples with and without glycerol were each dried in ambient conditions for two weeks and then post-cured at 120 °C for 2 h (with glycerol) or 90 min (without glycerol). Sinusoidal forces were applied to rectangular samples within linear viscoelastic regions (strain = 0.05) at a constant frequency (1 Hz) as a function of temperature. Temperature ranges for analyses were -80 to 150 °C for samples prepared with glycerol, and 35 to 220 °C for samples prepared without glycerol. The heating rate was 2 °C/min for all samples.

Results and discussion

DSC of BSA and EWPs

We first evaluated the thermal transitions for aqueous solutions of BSA and EWPs using differential scanning calorimetry (DSC), given that thermal denaturation is the envisioned mechanism for solution-to-solid curing that can be achieved in HAPPI AMPD. DSC studies on BSA (35 wt% in DI water or pH 6.6 buffer) as well as EWPs (35 wt% in DI water) each showed endothermic transitions consistent with thermal denaturation (Figure 2). BSA in DI water shows a relatively broad transition with a peak at 58 °C followed by another transition starting at 77 °C. For BSA in pH 6.6 buffer, we observed a transition at 65 °C, and EWPs in DI water showed a single transition at ca. 85 °C. The DSC data was found to be consistent with other reports. For example, Murayama et al. reported two-step thermal denaturation of BSA (2 wt% in water) with loss of tertiary structures at 57 °C, and a change of α-helix and β-transitions around 75 °C, as determined by FT-IR analyses.[18] The thermal transitions were used to guide our experimental setup and printing parameters using HAPPI.

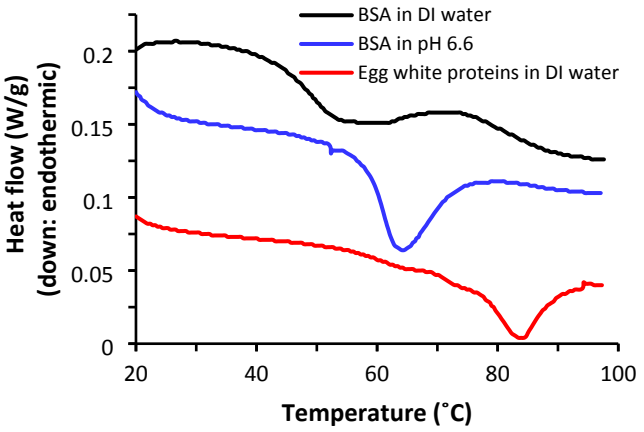

Figure 2 DSC thermograms of BSA in DI water, BSA in pH 6.6 and EWPs in DI water at 35 wt%.

HAPPI AMPD of aqueous BSA and EWPs resin formulations

We next moved into empirical evaluation of layer-by-layer formation of 3D structures using HAPPI AMPD. We used our HAPPI technology to generate patterned heat on a photothermal plate that served as the bottom of the resin vat. We evaluated two different approaches to HAPPI AMPD, one using a diode laser (808 nm) and another using a digital light processing (DLP) projector (Figure 3). The required BSA concentration for printability was 25-35 wt%. Below 25 wt%, we did not see reproducible structural integrity (fixity) during printing, and above 35 wt%, some protein did not dissolve. We also found that a 35 wt% solution of EWPs worked well in our

setups, giving homogeneous formulations and good fixity during printing. Furthermore, kinematic viscosities of a 35 wt% solution of BSA at 27 ˚C were measured to be 501 ± 3 cSt with glycerol and 123 ± 2 cSt without glycerol, which are suitable for vat-type 3D printing.

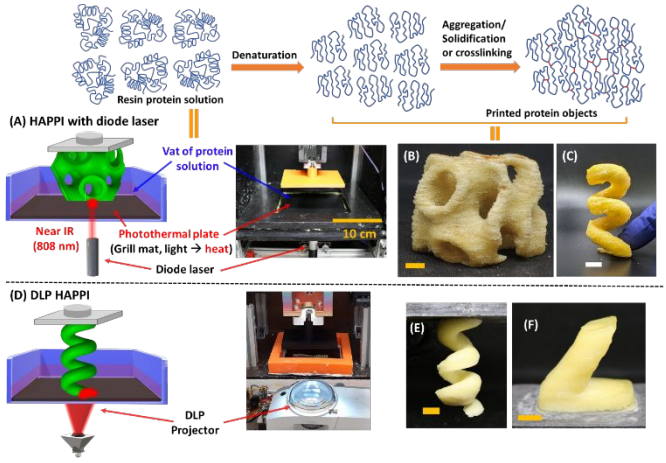

Figure 3 (A) simplified diagram of HAPPI with diode laser, (B) gyroid of BSA and (C) spiral of EWPs printed by HAPPI with diode laser, (D) DLP HAPPI, (E) spiral and (F) overhang of BSA printed by DLP HAPPI. (Scale bar = 1 cm).

Figure 3 shows a simplified diagram and actual image (Figure 3A) of the HAPPI printer with a diode laser (SLA-type setup), and representative products that were produced with this setup: a gyroid of BSA (Figure 3B) and a spiral of EWPs (Figure 3C). Figure 3D, 3E, and 3F depict the DLP HAPPI printer, as well as a spiral and overhang structure each printed by DLP HAPPI AM. In our previous studies, we found that application of a diode laser in HAPPI AM can achieve temperatures higher than 140 °C within seconds, suggesting this method was capable of thermal denaturation of proteins. The patterned heat leads to localized denaturation of proteins and solidification of protein material within the build layer. In HAPPI AMPD, we observed solidification of BSA solutions at temperatures close to the first transition in the denaturation process (58 °C).

In comparison with the temperatures that can easily be achieved with the laser setup, 58 °C is fairly low. We found that use of a safer, lower intensity DLP projector, in comparison with the diode laser, could also achieve the temperatures necessary for curing of the protein solutions. In DLP, the image for an entire layer is projected at once onto the photothermal plate, which results in lower local light intensity and heat generation compared with the laser-based setup. In general, we found that the diode laser, which provides much higher light intensity with better localization in comparison with the DLP setup, was better suited for AM of complex structures and gave higher resolutions of printed objects (as assessed visually). On the other hand, the DLP-based setup provided straightforward production of parts with simple geometries and offers a safer, more accessible option. A pH 6.6 buffer solution was selected as a solvent to increase the extent of denaturation upon heating, in comparison with results using a pH 7.4 solution.[19] Importantly, the pH should be maintained above 6.0 to avoid coagulation of the protein mixture.[20] A reducing agent, TCEP, was also added to increase the extent of denaturation via disruption of intramolecular disulfide bonds, which promotes unfolding of proteins.[19] We limited the concentration of TCEP to 15 mM to prevent pre-gelation at room temperature prior to printing.

To further investigate the properties of printed parts, we focused on BSA-based formulations to evaluate printing conditions, the effects of plasticizers, and the effects of thermal post-processing. Across the range of BSA concentrations, we found that the density of the dried printed parts was correlated with the wt% of BSA in the resin formulation. Before drying, the as-printed parts were found to have similar densities of 1.07, 1.04, and 1.11 g/cm^3 for resin solutions having 25, 30 and 35 wt%, respectively. After drying, the same parts had densities of 0.64, 0.68, and 0.76 g/cm^3, respectively (Figure 4A and Table 1). Upon seeing the ca. 30 – 40% reductions in densities, we expected formation of pores in the printed and dried specimens. To investigate, we analysed several specimens using SEM (Figure 4B, 4C and 4D) and found the parts to be highly porous. The average pore sizes were similar (ca. 200-µm diameter) for specimens produced with different wt% of BSA in the resin (Table 1). Qualitatively, based upon the SEM images, a greater number of open pores formed in parts made from 25 wt% solutions than those made from solutions containing higher wt% of BSA.

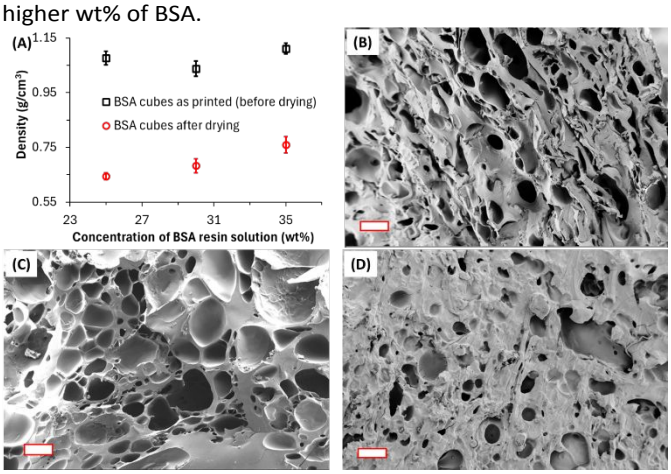

Figure 4 (A) Density of BSA cubes as printed or after drying at different concentrations of resin solution. Values represent an average of three experiments, error bars = 1 standard deviation. SEM cross-sectional image of a dried BSA cube printed from (B) 25, (C) 30 and (D) 35 wt% resin solution (scale bar = 300 µm).

Table 1 Density of BSA cubes as printed or after drying, and pore size of BSA across layers at different concentrations of resin solution.

Concentration of BSA resin solution (wt%)	Density (ρ) of BSA cubes (g/cm^3)[a]			Pore size (µm)[b]
	As printed	After drying	Δρ (%) after drying	
25	1.07 ± 0.03	0.64 ± 0.01	40 ± 2	195 ± 98
30	1.04 ± 0.03	0.68 ± 0.02	34 ± 2	247 ± 80
35	1.11 ± 0.02	0.76 ± 0.03	32 ± 2	178 ± 97

[a]Values represent an average of three experiments, error bars = 1 standard deviation. [b]Pore size as the longest distance was measured by ImageJ analysis on 45 pores in the SEM images of Figure 4.

We found similar results from SEM analysis of the side-on view of the layers within the specimen (Figure 5). In the side-on analyses, we found the average layer thickness increased with increasing wt% of BSA in the resin, from 130 to 161 to 285 µm as resin concentration increased from 25 to 30 to 35 wt% (Figure 6). The impact of drying the specimens does not appear to cause global shrinkage of the part, but instead creates layer spacings (resulting from layer shrinkage) and open pores throughout the part, which alters the density and potentially offers a means to produce bioplastic parts with tunable mesoscale architectures.

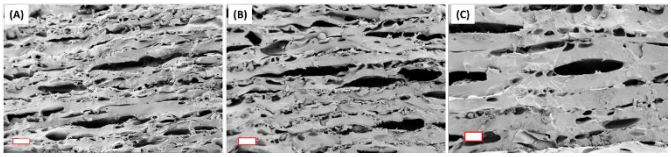

Figure 5 SEM cross-sectional images of a BSA cube printed from (A) 25, (B) 30 and (C) 35 wt% resin solution across layer lines (scale bar = 300 µm).

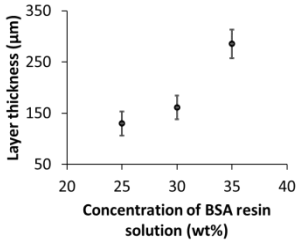

Concentration of BSA resin solution (wt%)	layer thickness (µm)
25	130 ± 24
30	161 ± 23
35	285 ± 28

Figure 6 Layer thickness of printed BSA at different concentrations of BSA resin solution. Values represent an average of three experiments, error bars = 1 standard deviation.

Assessment of mechanical properties

Thermal curing of proteins, which generally increases the extent of covalent crosslinking, is a primary method used to improve tensile properties of films of soy proteins[21] and whey protein,[13,14] as well as dogbone samples of BSA.[2] Since protein films tend to be brittle due to a combination of intermolecular disulfide bonding, hydrogen bonding, and hydrophobic interactions between protein chains, a plasticizer is often incorporated to reduce protein chain interactions and induce film flexibility.[22] Studies on proteins such as β-lactoglobulin and whey protein films showed that increasing the concentration of plasticizer increased elongation at break while decreasing tensile strength.[23,24] Those studies also showed that glycerol was an effective plasticizer for increasing elongation at break.

We evaluated the mechanical properties of HAPPI AMPD specimens using uniaxial tensile and compression tests, as well as dynamic mechanical analysis. Figure 7 and Table 2 show results from tensile tests on dogbones of BSA printed in aqueous media versus those printed in water-glycerol mixtures. Notably, although aqueous BSA formulations printed well in our HAPPI setup, we found the dogbone specimens to be too brittle for analysis after thermal post-curing. We did not analyse samples in their as-printed form from aqueous solutions because they were too soft for uniaxial tensile testing. Instead, hydration of the samples after thermal post-curing resulted in specimens that were suitable for analysis, which displayed an average Young's modulus of 119 ± 52 MPa and an average elongation at break of 40 ± 8%.

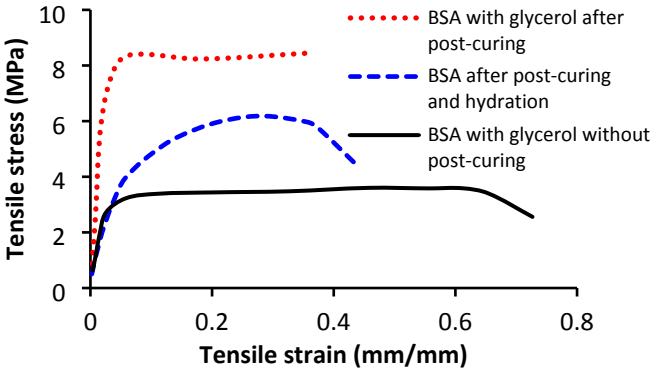

Figure 7 Results from tensile tests on dogbones of BSA with glycerol, BSA with glycerol after post-curing, and BSA after post-curing and hydration.

Table 2 Results from tensile tests on dogbones of BSA with glycerol, BSA with glycerol after post-curing, and BSA after post-curing and hydration.

	Young's modulus (MPa)	Ultimate strength (MPa)	Elongation at break (%)
BSA with glycerol after post-curing at 120 °C	233 ± 9	8 ± 1	31 ± 6
BSA after post-curing at 120 °C and hydration[a]	119 ± 52	7 ± 2	40 ± 8
BSA with glycerol without post-curing[b]	79 ± 17	4 ± 0.3	66 ± 7

[a]BSA samples that did not undergo post-curing were too weak to grip properly in the load frame for tensile testing. BSA samples after post-curing but without hydration were too brittle for tensile testing. [b]BSA samples with glycerol (printed from a solution using a water/glycerol mixture) were suitable for tensile testing.

Encouraged by the general printability of aqueous BSA formulations, yet seeking improved mechanical properties, we next analysed samples that were printed from water-glycerol mixtures. Here, the glycerol can act as a plasticizer for the cured protein. We found that dogbones of BSA printed with glycerol were suitable for mechanical analysis in their as-printed state and exhibited a Young's modulus of 79 ± 17 MPa and up to 66 ± 7% elongation at break (Figure 7, black). The ability to assess an elongation at break is a considerable improvement over the samples printed without glycerol, which could not be analysed due to the brittleness of the samples. Thermal post-curing did have a significant impact on the tensile properties of the specimens printed with glycerol, as expected, and several comparisons can be made. Parts made from BSA with glycerol after post-curing at 120 °C exhibited an almost 4-fold greater Young's modulus (233 ± 9 MPa) and 2-fold greater ultimate strength (8 ± 1 MPa) than those without post-curing (79 ± 17 MPa, 4 ± 0.3 MPa, respectively). Thermal post-curing reduced the elongation at break by more than 2-fold, from 66 ± 7% to 31 ± 6%. The increased modulus and strength after post-curing likely results from an increased degree of crosslinking among protein chains, which would also be consistent with the reduced elongation at break. Dogbones of BSA with glycerol after

thermal post-curing (Figure 7, red) exhibited an almost 2-fold greater Young's modulus (233 ± 9 MPa) compared to those without glycerol after post-curing (Figure 7, blue, 119 ± 52 MPa) and reached nearly the same elongation at break. In other words, the inclusion of glycerol can increase the tensile toughness of the parts. We also note that residual moisture content was largely consistent across all samples, regardless of thermal post-curing, and is therefore not likely the reason for the observed differences in mechanical properties.

Although we are unaware of direct comparisons for 3D printed proteins absent any chemical modification, it is worth noting similarities and differences with 3D printed parts made from acroylated BSA. Smith et al.[2] reported that increased elongation at break was achieved after tannic acid treatment of 3D-printed parts made from methacroylated BSA and various comonomers. The comonomers included poly(ethylene glycol) diacrylate (5 wt%, 75% elongation from 3D printed parts), acrylamide (3 wt%, 67% elongation from 3D printed parts), or 2-hydroxylethyl acrylate (2 wt%, 94% elongation from 3D printed parts). The elongation at break (66 ± 7%) of BSA printed via HAPPI AM with glycerol is comparable with those from their work while also displaying 5- to 10-fold higher Young's modulus.

The addition of glycerol and curing steps also changed the mechanical behaviour under uniaxial compression (Figure 8 and Table S1). Here, the cylindrical geometry of the specimens as well as the nature of the uniaxial compression setup allowed for evaluation of BSA parts as-printed, without glycerol in the formulation. Overall, the effect of post-curing was more significant in compressive properties than in tensile properties. Cylinders of BSA with glycerol showed a 10-fold greater compressive modulus (23 ± 0.6 MPa) than BSA without glycerol (2.3 ± 0.4 MPa). Post-curing increased the compressive modulus from 2.3 ± 0.4 MPa to 62 ± 9 MPa for BSA parts without glycerol, and from 23 ± 0.6 MPa to 60 ± 5 MPa for BSA parts with glycerol. Consistent with the tensile properties, increased modulus is attributed to increased degree of crosslinking after post-curing.

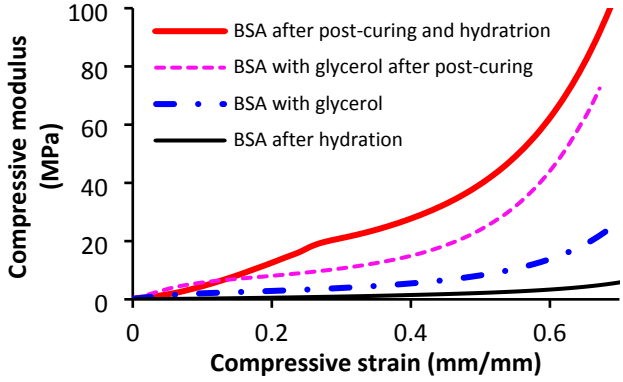

Figure 8 Results from compressive tests on cylinders of BSA with glycerol, BSA with glycerol after post-curing, and BSA after post-curing and hydration.

We also studied molecular relaxations of printed BSA parts as a function of temperature using DMA. The sample sets included parts produced with glycerol with and without thermal post-curing, as well as BSA parts from water with thermal post-curing but no hydration. Figure 9 and Table S2 show two transitions in the storage modulus (E') and tanδ peaks at ca. -45 and 70 °C. The lower temperature transition is attributed to secondary (or β) transitions induced by local motions including rotation of amino acid side groups linked to the main protein chain and internal motion within the side group.[25] The higher temperature transition is ascribed to a glass transition induced by global motion of the main chain. The β transitions of proteins were observed from -33 to -72 °C for extruded soy protein sheets[26] and from -35 to -52 °C for sunflower protein films[27] depending upon moisture content. Since the moisture content was consistent across our samples, we did not observe differences in storage modulus at room temperature nor secondary transition temperatures. Additionally, the storage modulus (E') of BSA after post-curing and no hydration at 40 ˚C was almost 7 times higher than that of BSA with glycerol. Additionally, the T_g of BSA with glycerol ranges from 70 to 80 °C whereas that of BSA after post-curing and no hydration was 123 °C. The combined tensile, DMA, and compression testing data indicate an ability to greatly modulate the mechanical behaviour of protein-based 3D printed parts. This parallels similar capabilities in photoresins used in vat photopolymerization that can be plasticized to soften the parts or thermally crosslinked in a post-curing step to increase strength and toughness.[2]

We further studied the crosslinking density (ν_e) of printed BSA with and without glycerol by DMA (Figure 9 and Table S2). The ν_e value is calculated from Eqn. 1 where $E'_{rubbery}$ is the storage modulus in the rubbery plateau regime (50 K above the T_g value at the tanδ peak), R is the universal constant and T is absolute temperature.[28] The ν_e of BSA samples with glycerol was found to be 0.58 kmol/m^3 without post-curing and 0.61 kmol/m^3 with post-curing. The ν_e of BSA samples with post-curing and no hydration was found to be 14.4 kmol/m^3, which is almost 24 times greater than with glycerol. These results show significant effects of plasticizers, such as glycerol, on calculated ν_e values as well as mechanical properties.

$$\nu_e = \frac{E'_{rubbery}}{(3RT)} \quad (1)$$

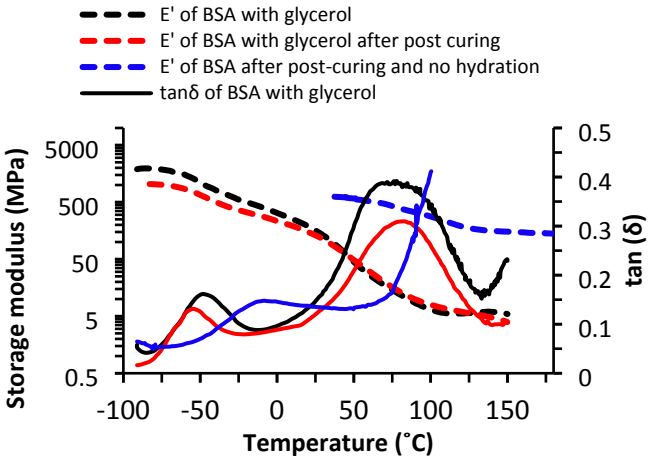

Figure 9 DMA results used to assess the storage modulus (E', dashed lines) and tanδ (solid lines) of BSA parts printed with glycerol, with (red) and without (black) thermal post-curing, and BSA parts with thermal post-curing and no hydration.

Aging studies

We observed that addition of glycerol increased the elongation at break while maintaining comparable Young's modulus and ultimate strength of the parts after post-curing. We were curious how the mechanical properties of BSA parts with glycerol would change over time since glycerol is not covalently bonded to BSA. Accordingly, we studied the impact of aging on the mechanical properties of dogbones produced from BSA with glycerol. Tensile tests of BSA with glycerol were conducted on two sets of specimens, one that did not undergo thermal post-curing and one that was post-cured at 120 °C. Samples were removed at 1-month intervals for 3 months (Figure 10, S1, and S2). We observed gradual changes in both the Young's modulus and elongation at break for each sample type. Without post-curing, we observed increases in Young's modulus from 79 ± 17 MPa to 140 ± 47 MPa and decreases in elongation at break from 66 ± 7% to 18 ± 9% over the course of 3 months. With thermal post-curing, aging resulted in decreased Young's modulus from 233 ± 9 MPa to 131 ± 14 MPa, and decreased elongation at break from 31 ± 6% to 20 ± 9%. Across all samples, the moisture content remained fairly consistent, between 10 to 13%, for the duration of the aging study (Table S3 and S4). We note that the Young's modulus, ultimate strength, and elongation at break within each type of sample became similar in value after 3 months (Figure 10, Table S3 and S4). This may be coincidental as well as only a temporary convergence, given that longer aging studies would be needed for application-specific assessment.

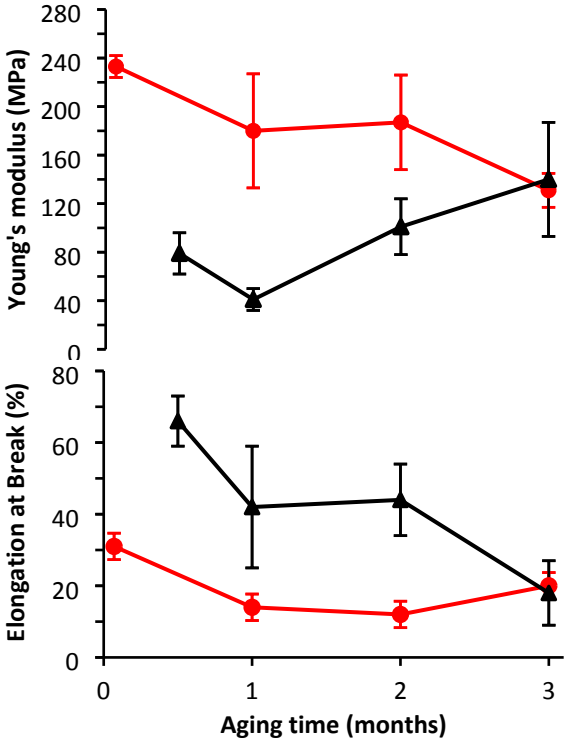

Figure 10 Comparison of Young's modulus (top) and elongation at break (bottom) of BSA dogbones with glycerol for sample that with (red circles) and without (black triangles) post-curing. Lines are for visual aid only. Values represent an average of three experiments, error bars = 1 standard deviation.

Biodegradation of BSA in pepsin solution

A potential benefit of using proteins without chemical modifications as build materials is their propensity for full biodegradation at the parts at their end of life. To investigate, we prepared sample discs (three groups of four discs: diameter = 16 ± 0.4 mm; height = 5.3 ± 0.2 mm; mass = 0.89 ± 0.01 g, 0.94 ± 0.005 g, and 0.96 ± 0.008 g after drying) and subjected half of them to thermal post-curing at 120 °C, and then observed their biodegradation in pepsin solution (pH 1.5 – 2.0) at 37 °C (Figure 11 and Table S5). The extent of biodegradation was determined gravimetrically, and we note that throughout the process there were small components of the sample specimens that broke free from the main part. We found that post-curing increased the time required to completely consume the discs, which had no visually observable solids by day 17. In contrast, samples that were not thermally post-cured achieved full consumption of solids within 13 days. Although more detailed comparative analyses are needed, our results suggest that unmodified proteins could degrade faster and more completely than chemically modified proteins. For example, reported biodegradation studies on 3D printed parts made from acroylated BSA, along with either poly(ethylene glycol) diacrylate (5 wt%) or acrylamide (3 wt%), showed ca. 61% degradation within 30 days.[2] We attribute the fast and complete degradation of our HAPPI AMPD samples to the absence of any comonomers or chemical modifications, as well as the processing conditions that involved replacing the pepsin solution every other day. Combining custom parts generated by HAPPI AMPD with full biodegradation could enable a circular economy of build materials.

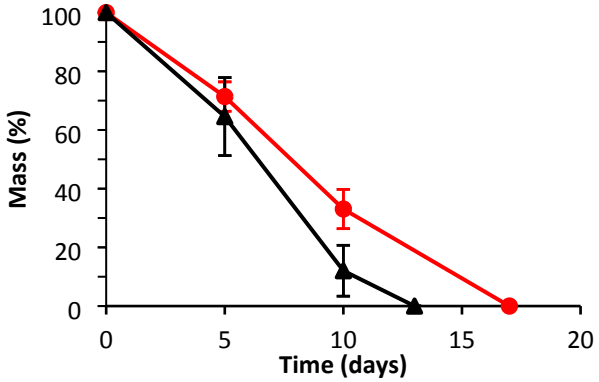

Figure 11 Degradation profiles of printed BSA cylinders with (red circles) and without (black triangles) thermal post-curing at 120 °C. Samples were prepared in pepsin solution, which was refreshed every other day. Mass % refers to the residual mass of solids as determined gravimetrically.

AMPD using photothermal particles in the formulation

Recognizing that the HAPPI AM technology is relatively new, and that the ability to cure proteins via thermal denaturation in AM could be generalizable, we considered using photothermal dyes in combination with familiar vat photopolymerization equipment designs that do not involve a photothermal plate. Our approach is inspired by Lear and co-workers' reports showing photothermal curing of silicone resin (Sylgard 184) facilitated by gold nanoparticles and irradiation with 532-nm laser light.[29] Photothermal particles within the resin rendered

the entire resin sensitive to photothermal transduction, thus enabling spatially resolved thermal curing. Similarly, we mixed our BSA solutions with bromothymol blue sodium salts (λ_{max} at 392 and 615 nm, data from commercial supplier) and attempted AMPD using DLP with a white light projector (Figure S3). Separately, we also incorporated IR-806 dye (λ_{max} at 806 nm, data from commercial supplier) for AMPD using a diode laser of 808 nm. We found that each setup was effective in achieving AMPD (Figure 12) with subjectively better surface finish and roughness from the DLP-based approach. Whether by laser rastering or DLP projection, AMPD can be implemented with common vat photopolymerization platforms having optically transparent vat bottoms, rather than photothermal plates.

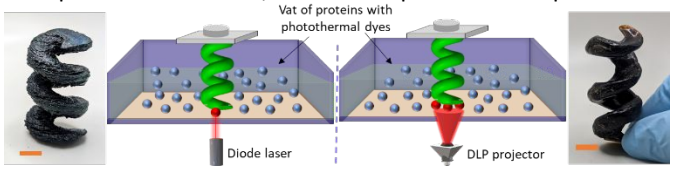

Figure 12 (Left) Simplified diagram of AMPD in a vat of proteins with photothermal dyes using a diode laser and a spiral of BSA with IR-806, (right) diagram using a DLP projector and a spiral of BSA with bromothymol blue. (Scale bar = 1 cm)

Conclusions

This study reports a new approach to AM that leverages protein denaturation and aggregation as the mechanism by which aqueous formulations are converted into solid parts. Two different AM techniques that enable patterning of heat via photothermal transduction were used in combination with BSA and EWPs to produce complex 3D structures, including gyroids with open voids and overhangs. Notably, the formulations have simple compositions, consisting of 25 – 35 wt% of protein in water, and the proteins do not require any chemical modifications to be printable into bioplastic parts. The mechanical properties of the printed products were tunable by post-curing and through the incorporation of a biodegradable plasticizer. Mechanical analyses revealed a Young's modulus up to 0.2 GPa, which is in the range of low-density polyethylene, and an elongation at break up to 70%, which is comparable to tannic acid-treated BSA. The printed bioplastics showed good enzymatic biodegradability and reached full degradation within 17 days. The results suggest a variety of applications including food products, nutritional supplements, packaging materials, and sustainable structural engineering materials. We anticipate that AMPD can be applied to other proteins, including plant-based variants, toward manufacturing of bioplastics with tunable mechanical properties from diverse sources.

Conflicts of interest

There are no conflicts to declare.

Data availability

The data supporting this article have been included as part of the Supplementary Information.

Acknowledgements

We are grateful to Prof. Alshakim Nelson (University of Washington) and Prof. Tina Wang (University of Wisconsin) for helpful discussions. A.J.B. acknowledges partial financial support from the Yamamoto Family, the Office of the Vice Chancellor for Research and Graduate Education at the University of Wisconsin-Madison with funding from the Wisconsin Alumni Research Foundation, as well as the Army Research Office (W911NF-20-2-0182-P00005-(76555-EG-MUR)) and Office of Naval Research (N00014-23-1-2499). The authors gratefully acknowledge the use of facilities and instrumentation at the UW-Madison Wisconsin Centres for Nanoscale Technology (wcnt.wisc.edu) partially supported by the NSF through the University of Wisconsin Materials Research Science and Engineering Center (DMR-1720415). Any opinion, findings, and conclusions or recommendations expressed in this material are those of the authors(s) and do not necessarily reflect the views of any funding agency or sponsor.

References

1 J. G. Rosenboom, R. Langer and G. Traverso, *Nat. Rev. Mater.*, 2022, **7**, 117.
2 P. T. Smith, G. Altin, S. C. Millik, B. Narupai, C. Sietz, J. O. Park and A. Nelson, *ACS Appl. Mater. Interfaces*, 2022, **14**, 21418.
3 P. T. Smith, B. Narupai, J. H. Tsui, S. C. Millik, R. T. Shafranek, D. H. Kim and A. Nelson, *Biomacromolecules*, 2020, **21**, 484.
4 E. Sanchez-Rexach, P. T. Smith, A. Gomez-Lopez, M. Fernandez, A. L. Cortajarena, H. Sardon and A. Nelson, *ACS Appl. Mater. Interfaces*, 2021, **13**, 19193.
5 T. Narancic, F. Cerrone, N. Beagan and K. E. O'Connor, *Polymers (Basel)*, 2020, **12**, 920.
6 T. D. Moshood, G. Nawanir, F. Mahmud, F. Mohamad, M. H. Ahmad and A. AbdulGhani, *Curr. Res. Green Sustain. Chem.*, 2022, **5**, 100273.
7 E. Álvarez-Castillo, C. Bengoechea, M. Felix and A. Guerrero, in *Bioplastics for Sustainable Development*, Springer Singapore, 2021, pp. 137–176.
8 J. Chen, T. Mu, D. Goffin, C. Blecker, G. Richard, A. Richel and E. Haubruge, *J. Food Eng.*, 2019, **261**, 76.
9 P. Phuhongsung, M. Zhang and B. Bhandari, *Food Res. Int.*, 2020, **137**, 109605.
10 Z. Liu, M. Zhang, B. Bhandari and Y. Wang, *Trends Food Sci. Technol.*, 2017, **69**, 83.
11 L. Liu, X. Yang, B. Bhandari, Y. Meng and S. Prakash, *Foods*, 2020, **9**, 164.
12 D. H. Song, V. B. Hoa, H. W. Kim, S. M. Khang, S. H. Cho, J. S. Ham and K. H. Seol, *Coatings*, 2021, **11**, 1344.
13 M. B. Perez-gago and J. M. Krochta, *J Food Sci*, 2001, **66**, 705.
14 M. B. Pérez-Gago, P. Nadaud and J. M. Krochta, 1999, *J. Food Sci*, 1999, **64**, 1034.
15 A. S. Beniwal, J. Singh, L. Kaur, A. Hardacre and H. Singh, *Compr. Rev. Food Sci. Food Saf.*, 2021, **20**, 1221.
16 C. U. Lee, K. C. H. Chin and A. J. Boydston, *ACS Appl. Mater. Interfaces*, 2023, **15**, 16072.
17 A. Boydston and C.-U. Lee, US Pat., US11597145B2, 2023.
18 K. Murayama and M. Tomida, *Biochemistry*, 2004, **43**, 11526.
19 A. J. R. Law and J. Leaver, *J Agric Food Chem*, 2000, **48**, 672.
20 N. Matsudomi, D. Rector and & J. E. Kinsella, *Food Chem.*, 1991, **40**, 55.
21 A. Gennadios, V. M. Ghorpade, C. L. Waller and M. A. Hanna, *ASABE*, 1996, **39**, 575.
22 M. Wihodo and C. I. Moraru, *J Food Eng*, 2013, **114**, 292.
23 N. B. Shaw, F. J. Monahan, E. D. O'Riordan and M. O'Sullivan, *J. Food Sci.*, 2002, **67**, 164.

24 R. Sothornvit and J. M. Krochta, *J Agric. Food Chem.*, 2000, **48**, 6298.
25 J. M. Bier, C. J. R. Verbeek and M. C. Lay, *Macromol. Mater. Eng.*, 2014, **299**, 524.
26 J. Zhang, P. Mungara and J. Jane, Mechanical and thermal properties of extruded soy protein sheets, *Polymer*, 2001, **42**, 2569.
27 A. Rouilly, A. Meriaux, C. Geneau, F. Silvestre and L. Rigal, *Polym. Eng. Sci.*, 2006, **46**, 1635.
28 G. Zhu, J. Zhang, J. Huang, X. Yu, J. Cheng, Q. Shang, Y. Hu, C. Liu, L. Hu and Y. Zhou, *Green Chem.*, 2021, **23**, 5911–5923.
29 R. Joseph Fortenbaugh and B. J. Lear, *Nanoscale*, 2017, **9**, 8555.

The data supporting this article have been included as part of the Supplementary Information.